Journal of Theoretical and Computational Acoustics
Vol. 26, No. 0 (2018) 1850025 (23 pages)

DOI: 10.1142/S2591728518500251

INTERNATIONAL ASSOCIATION
FOR MATHEMATICS AND
COMPUTERS IN SIMULATION

An Acoustic Hyperlens with Negative Direction Based on Double Split Hollow Sphere

Jung Sik Choi and Gil Ho Yoon*
School of Mechanical Engineering
Hanyang University, Seoul, Republic of Korea
**ghy@hanyang.ac.kr*
**gilho.yoon@gmail.com*

Received 21 March 2017
Accepted 29 March 2018
Published 12 July 2018

This study develops a new acoustic negative-refraction metamaterial that utilizes a synthesized double split hollow sphere (DSHS) for its unit cell. Recent relevant research has affirmed the concept that acoustic metamaterials can show unusual behavior that has not been observed in nature previously. However, as some hypothetical metamaterial designs have material properties not found in nature, the realization of practical metamaterials requires practical and complicated models. As a contribution to the development of acoustic metamaterials, the present study proposes a new anisotropic unit structure that encompasses Helmholtz resonators. This structure is referred to as the DSHS, is easy to manufacture, and has the advantage in that it uses the natural medium in its original form. By drawing the equifrequency or isofrequency contours of the designed two-dimensional (2D) anisotropic unit structure using the Floquet–Bloch's principle, the properties of the present metamaterial can be understood. Numerical simulations are also conducted to identify and present the characteristics of the presented acoustic metamaterial. Through these, a new refraction phenomenon is identified that deviates from Snell's law, and an acoustic hyperlens is numerically implemented that overcomes the diffraction limit.

Keywords: Acoustic metamaterial; hyperlens; double split hollow sphere; Floquet–Bloch's principle.

1. Introduction

Metamaterials have recently attracted increased attention from researchers in materials sciences, physics, mathematics, and engineering. Metamaterials are considered as a new class of composites, or as smart materials, with man-made subwavelength microstructures that show unusual behaviors that have not been observed or encountered in nature previously. Typically, metamaterials are arranged in repeating patterns at subwavelength scales, and their properties are not directly derived from the constituent material properties, but from their repeating unit cell patterns. Unit cell geometric shape, size, orientation and arrangement, are modified to achieve, among others, the enhancement, blocking, absorbing, or

bending of waves that are impossible to achieve with conventional, natural materials. In 1968, Veselago first presented a fundamental mathematical theory for possible metamaterials with negative electric permittivity and magnetic permeability, showing a backward wave medium propagation and a negative refractive index medium. After this pioneering research in electromagnetics, the possibility of synthesizing left-handed electromagnetic metamaterials that were not observed in nature was discussed by Smith *et al.*[1] In 2000, Pendry explored the concept of a perfect lens made of a left-handed metamaterial. An experimental verification of a negative refraction index was presented in Ref. 2. To the best of our knowledge, metamaterials also have some limitations, such as narrow optimal operating frequency bands, large spatial requirements owing to their repeating unit cells, and large energy losses owing to large impedance differences.[3–7] To overcome these limitations to make use of metamaterials in engineering applications, we can first refer to prior studies on this topic.[8–22]

The concepts of metamaterials were utilized to overcome the diffraction limits of ultrasonic and acoustic devices or superlenses.[8–10,21] A superlens is a lens that utilizes metamaterials that function beyond the diffraction limit. Until now, much of the pioneering superlens research has focused on electromagnetic wave applications (see Ref. 8 and references therein). Considering the analogy between acoustic and electromagnetic waves from the mathematical point-of-view, and considering the kinematics and the energy balance of wave propagation, some researchers have attempted to identify left-handed acoustic metamaterials with negative mass densities and/or a negative elastic moduli.[1,4,23] Such acoustic negative refractive index applications vary from a simple sound barrier to a complex device for nondestructive health monitoring and measurement devices. If these attempts succeeded, the resolutions of acoustic and ultrasonic devices would have been significantly improved. With this set objective, many relevant studies had been conducted subsequently.[9,10]

The resolution of an imaging system, such as a microscope, telescope, or camera, is proportional to the size of its objective and inversely proportional to the wavelength of light that is being observed. Additionally, there is a fundamental maximum to the resolution of any optical system owing to diffraction. This theoretical limit is known as Abbe's diffraction limit, described first by Ernst Abbe in 1873. The diffraction limit is defined by the following equation[24]:

$$D = \frac{\lambda}{2n\sin(\theta)}, \tag{1}$$

where D is the resolvable feature size, λ is the wavelength, n is the index of refraction of the medium, and θ is the half-angle subtended by the objective lens, respectively. As an illustrative example, two sound sources can be distinguished when the distance of the two sources is larger than the diffraction limit. This distance is dependent on their frequency and is equal to one-half of the wavelength (Fig. 1(b)). Conversely, when the distance between the two sources is smaller than the diffraction limit, the constituent sound waves far from the sources cannot be distinguished. In that case, they can be regarded as one sound source, as seen in Fig. 1(a).

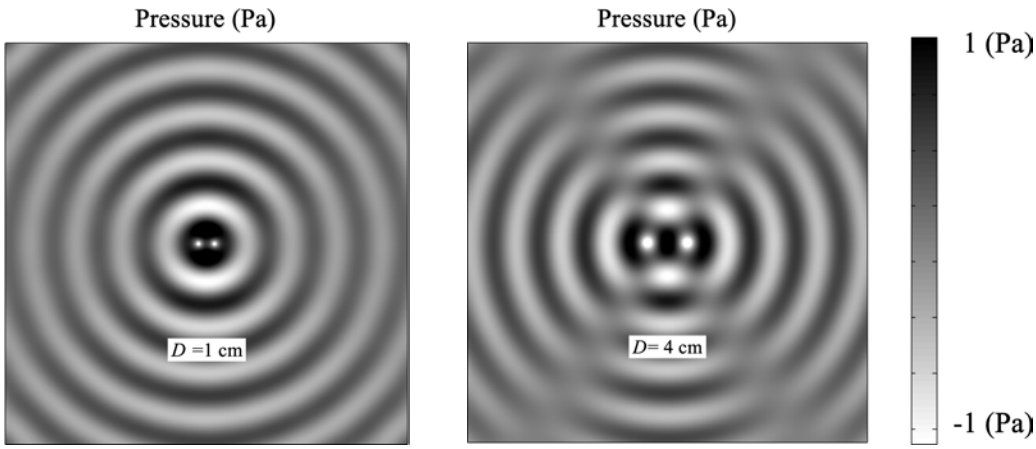

Fig. 1. Diffraction of sound sources ($\lambda = 5\,\text{cm}$, D: sound source distance). (a) $D = 1\,\text{cm}$ ($D < \lambda/2$) and (b) $D = 4\,\text{cm}$ ($D > \lambda/2$).

It is worth mentioning that waves in natural media cannot overcome Abbe's limit, as defined in Eq. (1). To overcome this limit with man-made materials or structures, the concept of a superlens or hyperlens has been proposed in many pioneering works.[8,9,11–13,21,25,26] To achieve these interesting characteristics, acoustic metamaterials exhibit negative refractions at the specific frequencies of sound sources.[8,25–27] For this purpose, many researchers have resorted to the use of man-made microstructures to achieve the apparent effect of negative mass density in acoustic metamaterials using mechanical resonators.[28–32] With the help of acoustic metamaterials, the effective mass density becomes frequency dependent, and acquires negative values in a certain frequency range. Acoustic metamaterials possess a negative effective modulus and have been proposed in various prior studies.[32,33] These acoustic metamaterials are man-made structures that have the form of a pipe with repeating lateral Helmholtz resonators or periodical membranes designed with side holes.[34] As these hyperlenses attenuate waves in one direction, waves perpendicular to that direction can propagate unencumbered by the diffraction limit, but with energy dissipation. Therefore, an acoustic metamaterial hyperlens provides an engineered solution to overcome the diffraction limit by transforming the evanescent wave. Extensive research has focused on the utilization of this interesting phenomenon in scientific and engineering applications, such as the imaging of subwavelength-sized objects.

There are two issues that are encountered in implementing the acoustic hyperlens for overcoming the diffraction limit. The first is to use materials with negative material properties. Since these materials are not present in nature, the acoustic hyperlenses are often theoretically or numerically implemented. The second issue is that the structure of the unit cells is complicated and difficult to fabricate. Generally, the acoustic hyperlenses are made by stacking many types of materials or by making unit cells of complex structure. These unit cells interfere with the actual implementation of the acoustic hyperlens.

In this study, we focus on the acoustic metamaterials of the local-resonance type, which are based on the double split hollow sphere (DSHS).[35] This DSHS structure has been used to realize acoustic metamaterials because it can be easily manufactured. Because this structure does not have negative material properties, its use to construct the unit cells of an acoustic hyperlens allows its realization using a medium that exists in nature.

This study is organized as follows. In the next section, we analyze the characteristics of DSHS. A new model that exhibits negative effective density is proposed and its dynamic characteristics are investigated. The wave propagation behavior of the one-dimensional (1D) system is subsequently studied and a new DSHS microstructure is introduced, based on the results of the 1D system. Numerical simulations on wave differentiation and propagation with negative refraction in acoustic metamaterials are subsequently presented. Finally, the findings are summarized and future research topics are briefly discussed.

2. DSHS as a Unit Lattice for an Acoustic Metamaterial System

2.1. *Acoustic hyperlens with negative density*

To develop a two-dimensional (2D) acoustic metamaterial structures, let us consider propagating waves in the circumferential (θ) and radial directions (r).

Without loss of generality, the wavevectors in the circumferential and the radial directions are denoted by k_θ and k_r, respectively. To realize a hyperlens, it is possible to consider a hyperlens evanescent wave in the circumferential direction with a passing wave in the radial direction.[36] In other words, to enable a hyperlens, the wave diffraction in the circumferential direction should be prevented by transforming the propagating wave in the circumferential direction to an evanescent wave. To describe the physical properties of the hyperlens, the equifrequency contour (EFC) curve can be considered for a certain frequency range.

In accordance to the wave propagation theory,[13,36] the EFC curve of an acoustic medium in the cylindrical coordinate system can be expressed as follows:

$$\frac{k_r^2}{\rho_r} + \frac{k_\theta^2}{\rho_\theta} = B^{-1}\omega^2, \tag{2}$$

where the effective density values in θ and r are denoted by ρ_θ and ρ_r, respectively. The bulk modulus of the media and the angular velocity are denoted by B and ω, respectively. Normally, in nature, all values of the variables in (2) are positive, and the EFC curves are limited to circular or parabolic shapes, depending on the magnitudes of ρ_θ and ρ_r. However, with the help of a man-made metamaterial structure, it is possible to obtain a negative value for ρ_θ and an imaginary value for k_θ. Figure 2(a) shows a hyperlens example with a hyperbolic curve in Fig. 2(b). For example, when the diffraction limit is 5 cm, sound sources separated by distances less than 5 cm cannot be distinguished. However, when thin layers with a positive density ($\rho_1 = 1000\,kg/\mathrm{m}^3$) and a negative density ($\rho_2 = -960\,\mathrm{kg/m}^3$) are juxtaposed in the radial direction, waves are transmitted, the hyperlens overcomes the diffraction limit, and the sound sources can be discriminated, as shown in Fig. 2(a). By

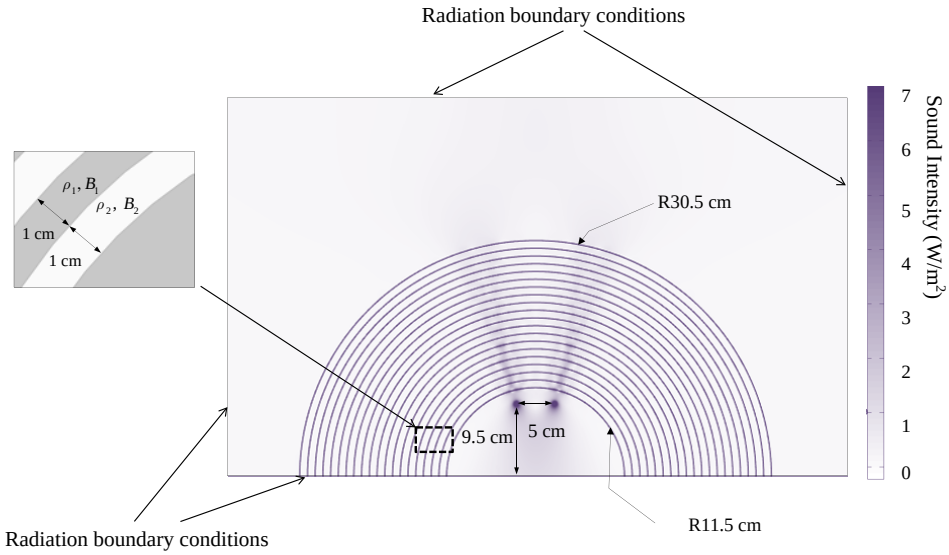

(a)

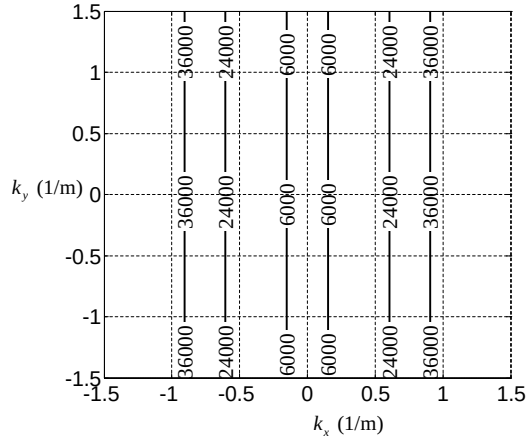

(b)

Fig. 2. Illustrative example of a hyperlens.[13] (a) Hyperlens with an acoustic metamaterial ($\rho_1 = 1000\,\mathrm{kg/m^3}$, $\rho_2 = -960\,kg/\mathrm{m}^3$, $B_1 = 2.22 \times 10^9\,\mathrm{N/m^2}$, $B_2 = 1.733 \times 10^9\,\mathrm{N/m^2}$, diffraction limit $\lambda = 5\,\mathrm{cm}$), and (b) EFC of the acoustic hyperlens in (a).

considering the volume ratios in the circumferential and the radial directions, the effective mass densities and the effective bulk moduli are also computed as follows:

$$\rho_r = f\rho_1 + (1-f)\rho_2, \quad \frac{1}{\rho_\theta} = \frac{f}{\rho_1} + \frac{1-f}{\rho_2}, \quad \frac{1}{B} = \frac{f}{B_1} + \frac{1-f}{B_2}, \tag{3}$$

where the volume ratio between the volumes of the first (V_1) and the second layers (V_2) can be expressed in accordance to $f(= V_1/(V_1+V_2))$. With these values, the EFC can be computed as shown in Fig. 2(b).

Although the above system was presented as a hyperlens,[13] it is impossible to realize it in practice because the density of the second layer is $\rho_2 = -960\,\mathrm{kg/m^3}$, which cannot be found in nature.

2.2. *Use of a unit model with DSHS structures for synthesis of an acoustic metamaterial*

In Fig. 2, the density of the second layer is set to have a negative value, and from an engineering point-of-view, this is impossible to realize in practice. Therefore, in order to realize this metamaterial and a hyperlens, it is necessary to introduce a man-made structure that has an effective negative density. In accordance to Eq. (2), the negative bulk moduli require one or more negative mass densities. In accordance to the definition of the acoustic hyperlens, Eq. (2) should be a hyperbolic equation. To satisfy the condition of achieving a negative bulk modulus and the condition for the synthesis of an acoustic hyperlens, one of the densities in Eq. (2) should be negative, or the wavevector of Eq. (2) should have an imaginary value. In Ref. 35, the DSHS structure has a negative bulk modulus and a positive mass density. In the case where the acoustic hyperlens uses a medium that exists in nature, the wavevector has an imaginary value because the mass density is always positive. In acoustics, an imaginary wavevector implies that the wave in the direction indicated by the vector is an evanescent wave. When the evanescent wave was generated in a specific direction, it cannot be propagated along this direction. The DSHS structure can block the wave based on a resonance phenomenon. This means that the evanescent wave is generated when a resonance phenomenon occurs. For this purpose, the present research employs the DSHS structure, as shown in Fig. 3. Because of the acoustic resonance inside the internal cavity, the realization of the acoustic metamaterial is possible. For a hyperlens, Eq. (2) should be a hyperbolic equation with a negative bulk modulus or a positive density. In Ref. 35, it was proven that the DSHS structure has a negative bulk modulus and a positive density.

The DSHS structure and the metastructures presented subsequently can be manufactured with modern manufacturing technologies, such three-dimensional (3D) printers or CNC machines. In Fig. 3, the DSHS structure has two masses and one spring. The subscripts "1" and "2" express the respective parameters of masses 1 and 2. Neglecting the effects of viscosity, the DSHS in Fig. 3 can be expressed by the mass–spring–mass system, and the relevant equation based on Newton's law can be formulated as follows:

$$\begin{aligned} m_{\mathrm{eff}} \frac{d^2 u_1}{dx^2} &= k(u_2 - u_1) + F, \\ m_{\mathrm{eff}} \frac{d^2 u_2}{dx^2} &= -k(u_2 - u_1) - F, \end{aligned} \tag{4}$$

where x is the displacement, u and p denote the acoustic pressure, and $F(= Sp)$ is the external force. Assuming harmonic oscillations for the pressure ($p = p_0 e^{i\omega t}$) and the displacement ($u = u_0 e^{i\omega t}$), and given that the relationship between the two displacements is

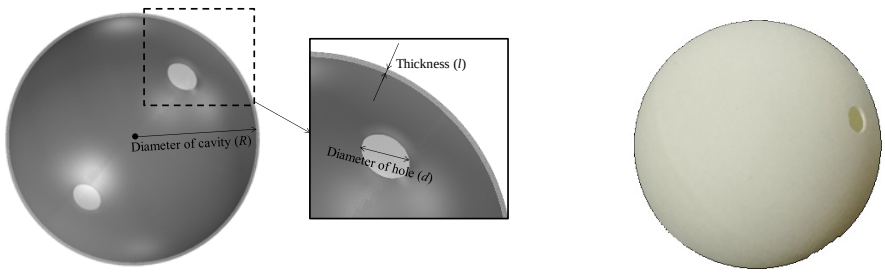

(a)

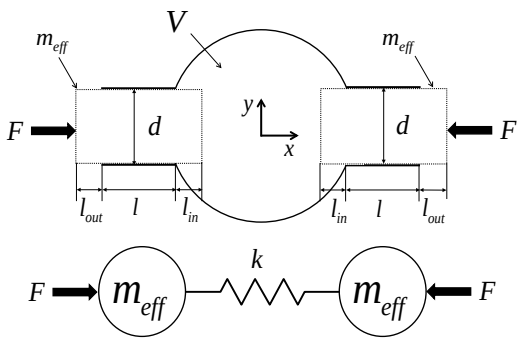

(b)

Fig. 3. DSHS structure: (a) 3D model of DSHS and its practical realization and (b) geometry of DSHS.

$u = u_2 - u_1$, the governing equation in (4) can be further formulated as

$$\begin{aligned} &-\omega^2 m_{\text{eff}} u_1 = k(u_2 - u_1) + Sp, \quad -\omega^2 m_{\text{eff}} u_2 = -k(u_2 - u_1) - Sp, \\ &\begin{bmatrix} k - m\omega^2 & -k \\ -k & k - m\omega^2 \end{bmatrix} \begin{Bmatrix} u_1 \\ u_2 \end{Bmatrix} = \begin{Bmatrix} Sp \\ -Sp \end{Bmatrix}. \end{aligned} \tag{5}$$

If $u = u_2 - u_1$ expresses the relationship between the two displacements, the governing equation in (5) can be simplified as follows:

$$-m_{\text{eff}}\omega^2 u = -2\rho c^2 \frac{S^2}{V} u - 2Sp. \tag{6}$$

The effective mass is $m_{\text{eff}} = \rho S l_{\text{eff}}$, and the effective neck length is $l_{\text{eff}} = l_{\text{in}} + l + l_{\text{out}}$, where S is the sectional neck area. The bulk modulus, the density, and the volume of the internal cavity are set to B, ρ, and V, respectively. By assuming harmonic oscillations for the pressure ($p = p_0 e^{i\omega t}$), the governing equation in (6) can be further formulated in accordance to,

$$Sp_0 = -\rho c^2 \frac{S^2}{V} u_0 + \frac{1}{2}\omega^2 \rho S l_{\text{eff}} u_0 = -\frac{\rho S l_{\text{eff}}}{2} \left(\frac{2c^2 S}{V l_{\text{eff}}} - \omega^2 \right) u_0 \tag{7}$$

with $\omega_0 = c\sqrt{2S/(l_{\text{eff}}V)}$, for which Eq. (7) can be further simplified to

$$p_0 = -\frac{\rho l_{\text{eff}}}{2}(\omega_0^2 - \omega^2)u_0. \tag{8}$$

Correspondingly, the displacement u_0 can be obtained as

$$u_0 = -\frac{2p_0}{l_{\text{eff}}(\omega_0^2 - \omega^2)\rho}. \tag{9}$$

Equation (9) has many similarities with the Helmholtz resonator, and this DSHS structure has almost the same characteristics as this resonator type. This study uses the DSHS structure as the unit cell of the acoustic metamaterial structure. The next section constructs a 2D mass and a spring system to use this DSHS unit structure.

2.3. *Analytical calculation of the dispersion relation of an equivalent mass–spring lattice for acoustic metamaterials*

The previous section presented a DSHS unit system with a generated evanescent wave in the intended wave propagation direction for a particular frequency range. It is important to realize the referred unit cells in an acoustic metamaterials structure. For the sake of the realization of an acoustic metamaterial structure, we re-investigate the unit 2D mass–spring lattice system of Fig. 4, which converts a propagating wave to an evanescent wave in the circumferential direction (θ). Without loss of generality, the displacements in the circumferential and radial directions of mass m_1 at the nth and the jth layers are denoted by $u_\theta^{n,j}$ and $u_r^{n,j}$, respectively. The displacements of mass m_2 at the nth and the jth layers are denoted by $\nu_\theta^{n,j}$ and $\nu_r^{n,j}$, respectively. The circumferential and radial distances between the masses m_1 are d_θ and d_r, respectively. The above 2D mass–spring lattice system has been used to construct the metamaterial and shows the characteristics of many hyperlens systems. In our study, we reinvestigate this system to present a metamaterial system with DSHS unit systems.

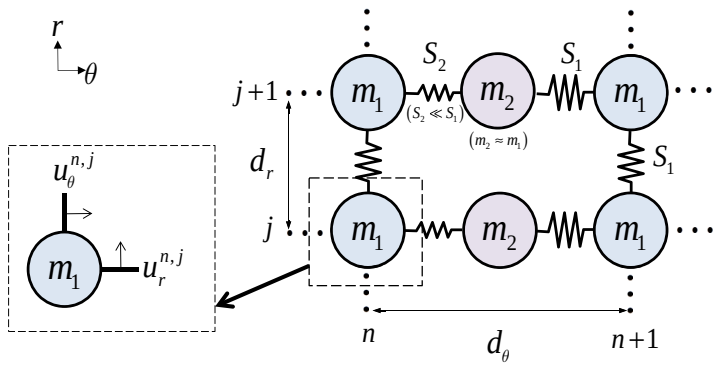

Fig. 4. Unit 2D mass–spring lattice.

In accordance to Newton's law, the governing equations of the unit cell in Fig. 4 in the θ-direction can be written as follows:

$$m_1 \frac{\partial^2 u_\theta^{(n,j)}}{\partial^2 t} = S_2(\nu_\theta^{(n,j)} - u_\theta^{(n,j)}) - S_1(u_\theta^{(n,j)} - \nu_\theta^{(n-1,j)}), \tag{10}$$

$$m_2 \frac{\partial^2 \nu_\theta^{(n,j)}}{\partial^2 t} = S_1(u_\theta^{(n+1,j)} - \nu_\theta^{(n,j)}) - S_2(\nu_\theta^{(n,j)} - u_\theta^{(n,j)}), \tag{11}$$

$$\begin{aligned} u_\theta^{(n+1,j)} &= e^{-ik_\theta d_\theta} u_\theta^{(n,j)}, \quad u_\theta^{(n-1,j)} = e^{ik_\theta d_\theta} u_\theta^{(n,j)}, \\ \nu_\theta^{(n+1,j)} &= e^{-ik_\theta d_\theta} \nu_\theta^{(n,j)}, \quad \nu_\theta^{(n-1,j)} = e^{ik_\theta d_\theta} \nu_\theta^{(n,j)}. \end{aligned} \tag{12}$$

Assuming harmonic motion, $u_\theta^{(n,j)} = u_0 e^{i(\omega t - k_\theta r_\theta)}$ and $\nu_\theta^{(n,j)} = \nu_0 e^{i(\omega t - k_\theta r_\theta)}$ (where u_0 and ν_0 are arbitrary numbers, and r_θ is the distance in the θ-direction), and considering Floquet's theory (12), the following governing equations can be obtained:

$$-\omega^2 m_1 u_\theta^{(n,j)} = S_2(\nu_\theta^{(n,j)} - u_\theta^{(n,j)}) - S_1(u_\theta^{(n,j)} - e^{ik_\theta d_\theta} \nu_\theta^{(n,j)}), \tag{13}$$

$$-\omega^2 m_2 \nu_\theta^{(n,j)} = S_1(e^{-ik_\theta d_\theta} u_\theta^{(n,j)} - \nu_\theta^{(n,j)}) - S_2(\nu_\theta^{(n,j)} - u_\theta^{(n,j)}). \tag{14}$$

Alternatively, these equations can be expressed in a matrix form as

$$\begin{bmatrix} (S_1 + S_2) - \omega^2 m_1 & -(S_2 + S_1 e^{ik_\theta d_\theta}) \\ -(e^{-ik_\theta d_\theta} S_1 + S_2) & (S_1 + S_2) - \omega^2 m_2 \end{bmatrix} \begin{bmatrix} u_\theta^{(n,j)} \\ \nu_\theta^{(n,j)} \end{bmatrix} = \mathbf{0}. \tag{15}$$

The dispersion relationship can be obtained by solving the eigenvalue problem of (15) as follows:

$$-m_1 m_2 \omega^4 + (m_1 + m_2)(S_1 + S_2)\omega^2 = 2S_1 S_2(1 - \cos(k_\theta d_\theta)), \tag{16}$$

$$\cos(k_\theta d_\theta) = \frac{2S_1 S_2 + m_1 m_2 \omega^4 - (m_1 + m_2)(S_1 + S_2)\omega^2}{2S_1 S_2}. \tag{17}$$

To achieve an imaginary wave number k_θ, or an evanescent wave, the following condition should be satisfied:

$$\text{Condition 1:} \quad \frac{2S_1 S_2 + m_1 m_2 \omega^4 - (m_1 + m_2)(S_1 + S_2)\omega^2}{2S_1 S_2} < -1, \tag{18}$$

$$\text{Condition 2:} \quad \frac{2S_1 S_2 + m_1 m_2 \omega^4 - (m_1 + m_2)(S_1 + S_2)\omega^2}{2S_1 S_2} > 1. \tag{19}$$

If an angular frequency ω is chosen to satisfy conditions (18) or (19), the wavevector k_θ becomes a pure imaginary value, or the wavevector acquires a negative value. The left-hand

sides of the above equations can be rewritten in a summarized form as

$$1+\frac{m_1m_2\omega^4}{2S_1S_2}-\frac{(m_1+m_2)(S_1+S_2)\omega^2}{2S_1S_2}$$

$$=1+\frac{1}{2}\left(\sqrt{\frac{m_1}{S_1}}\right)^2\left(\sqrt{\frac{m_2}{S_2}}\right)^2\omega^4-\frac{(m_1+m_2)\left(1+\dfrac{S_2}{S_1}\right)\omega^2}{S_2}. \tag{20}$$

Applying the conditions $S_2 < S_1$, $\omega_1 = \sqrt{S_1/m_1}$ and $\omega_2 = \sqrt{S_2/m_2}$ to the above equation leads to,

$$1+\frac{1}{2}\left(\frac{\omega}{\omega_1}\right)^2\left(\frac{\omega}{\omega_2}\right)^2-\frac{(m_1+m_2)\omega^2}{S_2}. \tag{21}$$

Since the angular frequency ω is small, ω/ω_1 and ω/ω_2 are smaller than 1. Thus, the ω^4 term can be neglected. In the actual model in Fig. 6, the coefficient of ω^4, namely, $\frac{1}{2}(\frac{1}{\omega_1\omega_2})^2$, is equal to 6×10^{-15}, whereas the coefficient of ω^2, $\frac{(m_1+m_2)}{S_2}$, is 1.14. Therefore, the coefficient of ω^4 is much smaller than the coefficient of ω^2, and the ω^4 term can be neglected.

Furthermore, if the stiffness value S_2 is much smaller than S_1, as shown in Fig. 5, then the above conditions can be further simplified as follows:

$$\cos(k_\theta d_\theta)\cong\frac{2S_2-(m_1+m_2)\omega^2}{2S_2}. \tag{22}$$

Alternatively, Eq. (22) can be derived by assuming $u_\theta^{(n,j)} = \nu_\theta^{(n,j)}$ based on the posed assumptions in Fig. 5. Equations (13) and (14) can then be written as follows:

$$-\omega^2m_1u_\theta^{(n,j)}=-S_2(u_\theta^{(n,j)}-e^{ik_\theta d_\theta}u_\theta^{(n,j)}),\quad -\omega^2m_2u_\theta^{(n,j)}=S_2(e^{-ik_\theta d_\theta}u_\theta^{(n,j)}-u_\theta^{(n,j)}). \tag{23}$$

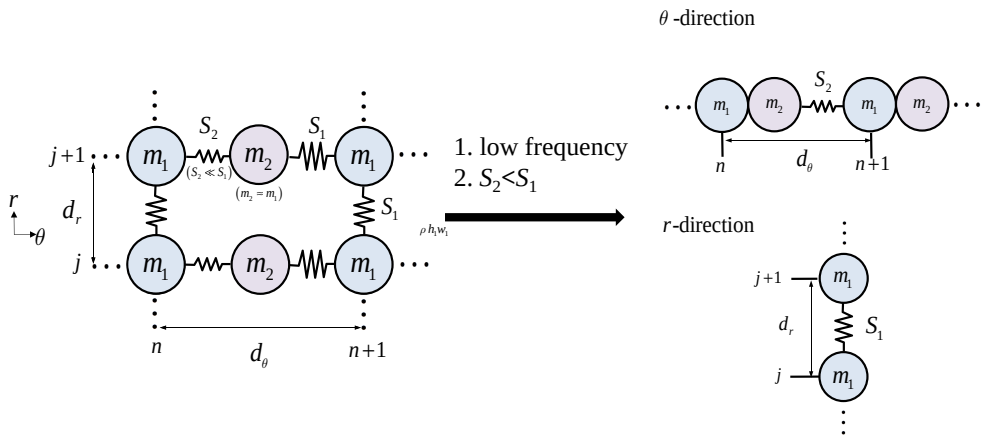

Fig. 5. Working principle of the DSHS in the circumferential and the radial directions.

Addition of the two equations in (23), the following equation can be derived,

$$-\omega^2(m_1+m_2)u_\theta^{(n,j)} = -2S_2u_\theta^{(n,j)} + S_2(e^{ik_\theta d_\theta} + e^{-ik_\theta d_\theta})u_\theta^{(n,j)}$$
$$= -2S_2(1-\cos(k_\theta d_\theta))u_\theta^{(n,j)}. \tag{24}$$

All the parameters of the above equation have positive values. In order to realize a metamaterial structure with imaginary wavevectors, the following conditions should be optimized.

$$\omega > 2\sqrt{\frac{S_2}{m_1+m_2}}, \tag{25}$$

$$\cos(k_\theta d_\theta) = \frac{2S_2-(m_1+m_2)\omega^2}{2S_2} < -1. \tag{26}$$

By (24)–(26), the circumferential wavevector k_θ acquires a pure imaginary value in specific frequency range.

2.4. *Acoustic metamaterial system with DSHS structures*

It is possible to engineer an acoustic metamaterial equivalent to the lattice model in Fig. 4. In Sec. 2.2, the DSHS system is defined as a 1D mass–spring system. Based on the definition of the hyperlens, the hyperlens structure must be based on anisotropic material properties. Therefore, to realize an acoustic hyperlens with a DSHS system, an anisotropic mass–spring system should be designed. However, as the acoustic masses and the acoustic springs should be realized, this would require a complex geometry. To simplify the problem, we have noticed in the previous section that the stiffness value of S_2 is much smaller than S_1, thereby allowing the possible simplification of the wave equation in the circumferential direction, as illustrated in Fig. 5. In other words, the spring with stiffness S_1 can be regarded as a rigid bar in the circumferential direction. We thus present the following acoustic metamaterial in which the circumferential wave cannot propagate, in comparison to the radial wave that can propagate. From an acoustics point-of-view, the neck of the resonator represents a corresponding mass, and the cavity of the resonator represents a spring. Therefore, the mass–spring system in Fig. 5 can be realized by the acoustic system in Fig. 6.

The acoustic hyperlens system in Fig. 6(b) is not uniform in any layer because the shape of DSHS is spherical. However, if this layer is laminated, each layer has the same shape. Therefore, this acoustic system can be uniform in the z-direction, and this acoustic system can be considered as a 2D system. Without loss of generality, the following values are used for the geometric parameters considering the overall size of the acoustic metamaterial hyperlens. The equivalent masses and the springs of the acoustic metamaterial hyperlens can thus be expressed as follows:

$$m_1 = \rho h_1 w_1, \quad m_2 = \rho h_1 w_1, \quad S_1 = \frac{\rho c^2 w_1}{(h_4 w_4)}, \quad S_2 = \frac{\rho c^2 h_2}{(h_3 w_3)}, \tag{27}$$

$$\omega_{\text{resonance-radial}} = \sqrt{\frac{S_1}{m_1}}, \quad \omega_{\text{resonance-circumferential}} = \sqrt{\frac{S_2}{m_1+m_2}}. \tag{28}$$

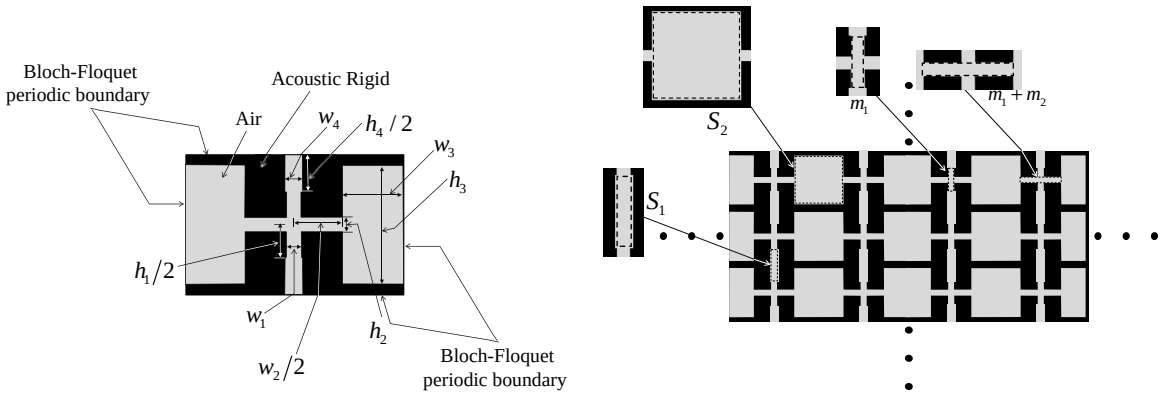

(a) (b)

Fig. 6. Unit lattice of an acoustic metamaterial hyperlens using DSHS: (a) unit lattice ($h_1 = 1.1 \times 10^{-2}$ m, $h_2 = 1/3 \times 10^{-2}$ m, $h_3 = 4 \times 10^{-2}$ m, $h_4 = 4 \times 10^{-2}$ m, $w_1 = 0.25 \times 10^{-2}$ m, $w_2 = 1.65 \times 10^{-2}$ m, $w_3 = 4 \times 10^{-2}$ m, $w_4 = 5 \times 10^{-2}$ m, air density = 1.24 kg/m^3, air sound speed = 343 m/s), (b) acoustic metamaterial using unit lattice with mass-spring system of Fig. 5.

It is then found that use of the geometric values listed in Fig. 6 that the resonant frequencies of the radial and the circumferential directions of the unit lattice in Fig. 6 are approximately 5170 Hz and 3854 Hz, respectively. In the dispersion equation, the wave propagation can be defined in accordance to Eq. (2). In terms of material mechanics, media in nature cannot have negative mass densities. Based on the definition of the hyperlens, the shape of EFC must be hyperbolic. Therefore, in the case of the hyperbolically shaped EFC represented by Eq. (2), as shown in Fig. 7(b), the wavenumber k_θ should acquire imaginary values. This means that the wave along the r-direction is always a propagation wave, and

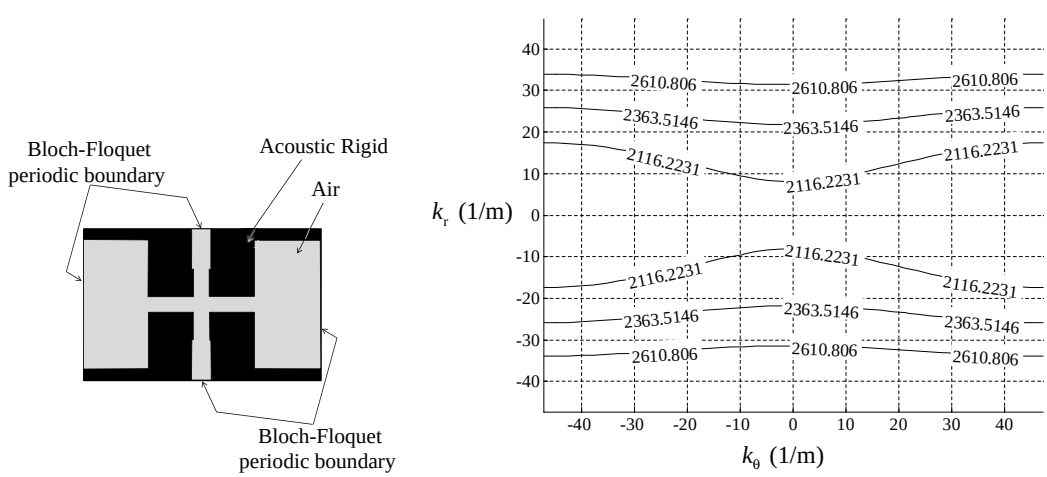

(a) (b)

Fig. 7. EFC of the present unit cell. (a) FE simulation conditions and (b) EFC contour.

the wave along the θ-direction is always an evanescent wave. This is because the wave along the θ-direction cannot appear even though it always occurs in the r- and θ-directions. In addition, the function of the hyperlens is improved when the EFC is parallel to the k_θ axis because the wave always propagates in the r-direction. Comparing these frequency values, it can be concluded that the performance of the hyperlens at 2600 Hz is not related to the fundamental frequencies of the radial and the circumferential directions (Bragg gap or scattering).

All the simulations were completed using the commercial software (COMSOL).

3. Numerical Simulations of Acoustic Metamaterials

3.1. *Negative refraction with an acoustic metamaterial*

In the previous section, the unit cell of the acoustic hyperlens was approximated by the 2D anisotropic mass–spring system and its excitation frequency range was analyzed using the EFC. The acoustic hyperlens has characteristic of negative refraction. Before implementing the acoustic hyperlens, the negative refraction characteristics should be verified. To show the applicability of the present acoustic metamaterial, a negative refraction example is considered in Fig. 8. Note that the unit structure in Fig. 7 is repeated and assembled to construct the metamaterial array. The plane wave input condition ($p = 1\,\mathrm{N/m^2}$, 2600 Hz) is defined at the left lower part, and no-reflection boundary conditions are assigned at the external boundaries. The geometric dimensions are chosen to show the performance of the present acoustic metamaterial structure. The upper and lower areas of the acoustic metamaterial structure are filled by air, and the acoustic metamaterial structure is assumed to be a rigid body.

To explain the results, Fig. 8 is separated in three layers, namely, in a bottom, middle, and an upper layer. The middle layer refers to the metamaterial's area, while the area

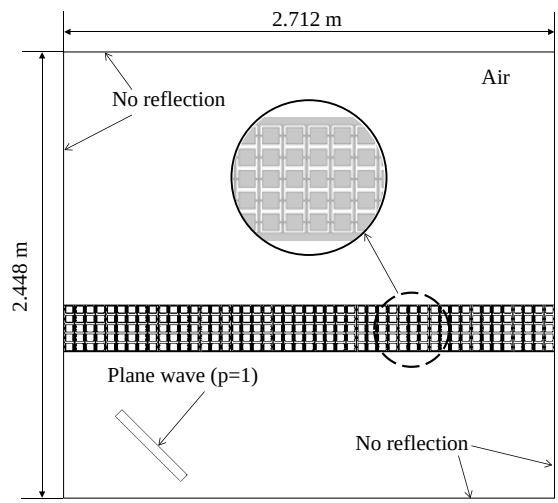

Fig. 8. Modeling and boundary conditions for a negative refraction acoustic metamaterial structure.

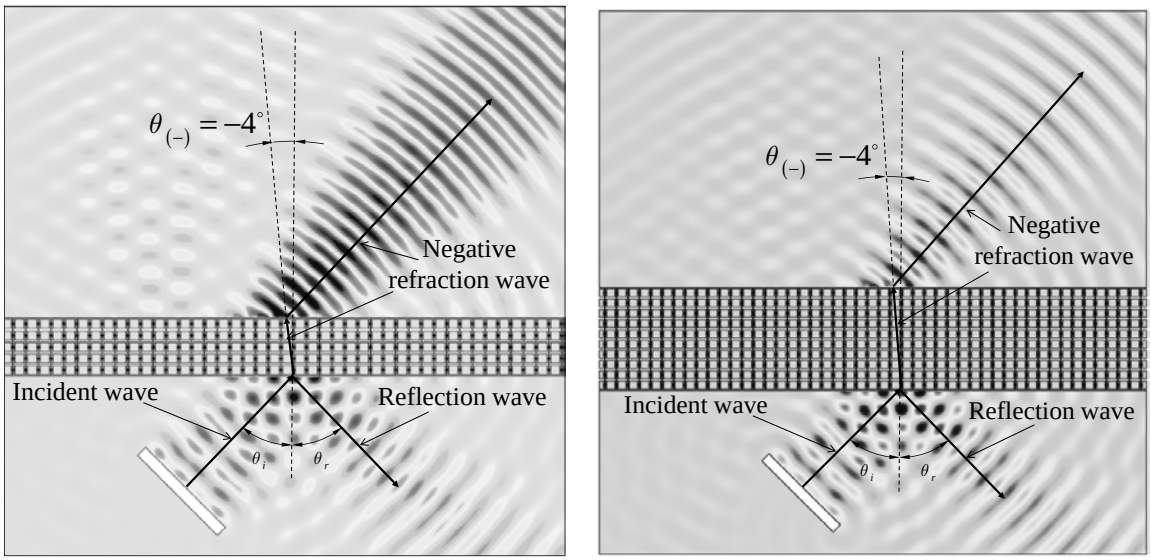

(a) (b)

Fig. 9. Negative refraction simulations at 2600 Hz with (a) 5 layers and (b) 10 layers.

below it is the bottom layer, and the area above it is the upper layer. Figure 9 shows the two simulation results with 5 layers and 10 layers. The incident (θ_i) and the reflected angles (θ_r) are 45°. The manually measured transmitting wave angle $\theta_{(-)}$ is approximately −4°. From Snell's law, the refraction index can be calculated in accordance to

$$n_2 = n_1 \frac{\sin\theta_i}{\sin\theta_r}. \tag{29}$$

The incident angle (θ_i) and the reflected angle (θ_r) are 45°. The manually measured transmitting wave angle $\theta_{(-)}$ is approximately −4°. From Snell's law, the refractive index of the acoustic metamaterial structure is approximately $n_{\text{hyper}} = -10.137$, thereby showing negative refraction in the middle layer. Based on Eq. (2), the negative refraction phenomenon occurs when only one wavevector acquires imaginary values because the wave direction has to reverse in that case. Therefore, in accordance to Fig. 9, the wavevector in the x-direction is imaginary owing to the DSHS, while the wavevector in the y-direction is real. As expected, the wave in the x-direction is an evanescent wave owing to the DSHS array that acquires imaginary values, and the wavevector in the x-direction that has nonzero real numbers. Conversely, the wave in the y-direction is real and can propagate.

Note that by increasing the number of layers, the amplitude of the transmitted wave decreases, but the transmitted wave angle ($\theta_{(-)}$) is not significantly altered. Figure 10 shows three simulation results at different incident wave angles, namely, at 50°, 55°, and 60°. Interestingly, the transmitted wave angles vary from −2.5°, 0°, and 3.3°, respectively. This is owing to the anisotropic characteristics of the metastructure. The unit cell of the acoustic hyperlens was approximated by the 2D anisotropic mass–spring system, and the driven

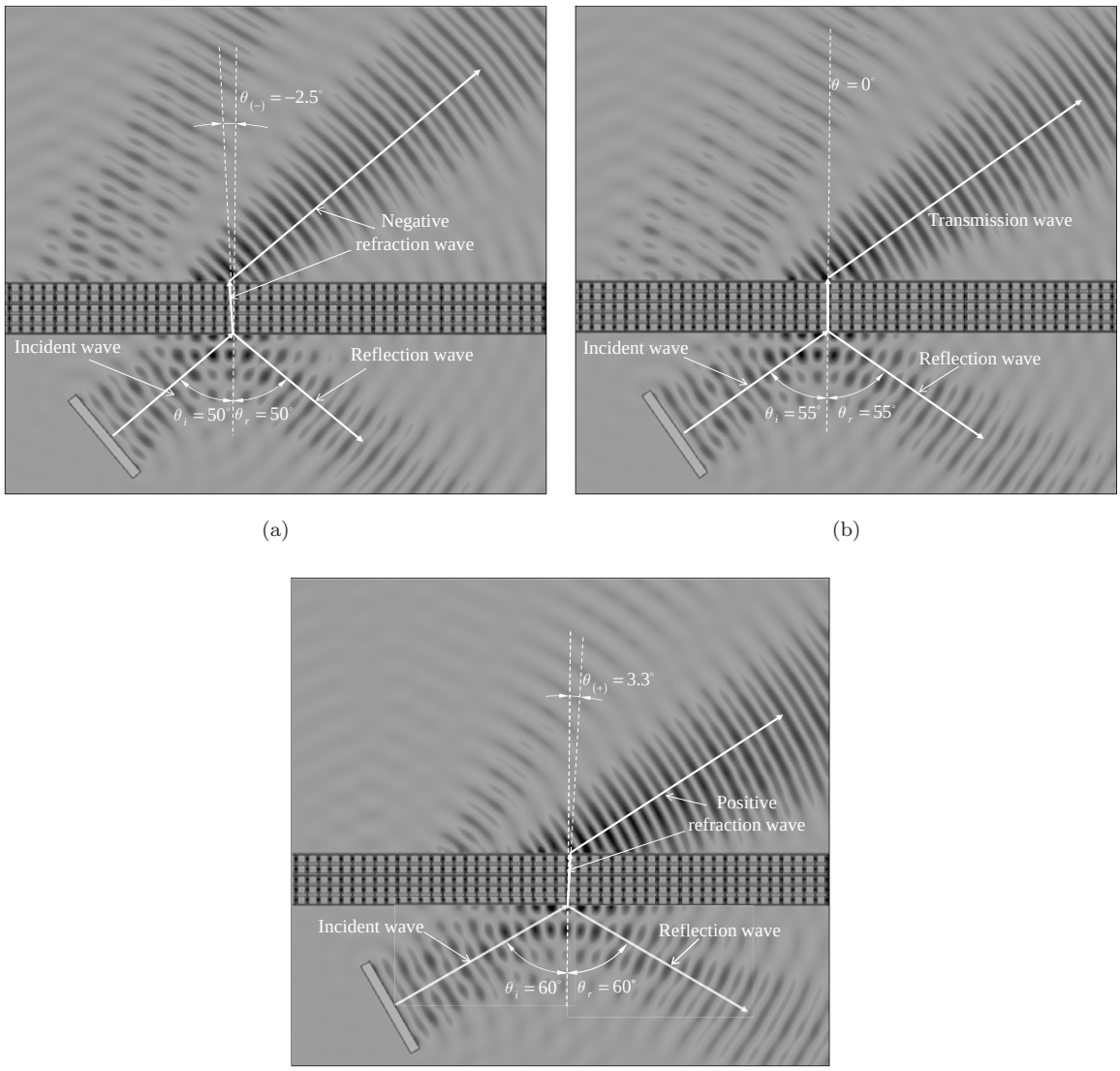

Fig. 10. Refraction angle with respect to different incident angles for an incident wave at a frequency of 2600 Hz.

frequency range of the metastructure was analyzed using the EFC. Before implementing an acoustic hyperlens with negative refraction, the following example shows the characteristics of the negative refraction of the present metastructure and derives the relationship between the angles of the incident and refracted waves using EFC analyses.

The EFC that shows the propagating wave direction can explain these anisotropic characteristics. The wave propagates in the perpendicular direction to the EFC contour. Figure 11 shows the EFC contour with the same incident angles as those in Fig. 10. The lattice constants in the x- and the y-directions are a and b, respectively. The wavevector can be

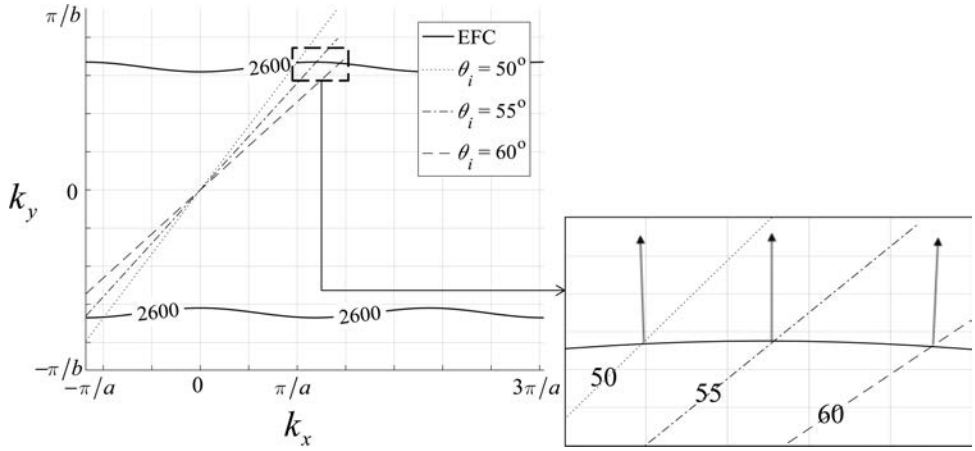

Fig. 11. EFC at different incident angles. The dotted lines represent the directions of the incident wave. The arrows in the expanded figure of the EFC represent the directions of the diffraction wave.

decomposed into x and y components using the incident angles to construct a straight line in k-space. As shown in Fig. 11, the transmitted angles in the present acoustic metamaterial of $-1.9°$, $-0.3°$, and $2.6°$, can be obtained by first finding the intersection of the line in k-space with the EFC, and by determining the angle of the k-space vector that is perpendicular to the EFC at the point of intersection, thus matching the results shown in Fig. 10.

In addition, Fig. 12 shows the relationship between the negative refractive index and the excitation frequency. In Fig. 10(b), a transmitted angle with a value of zero is observed

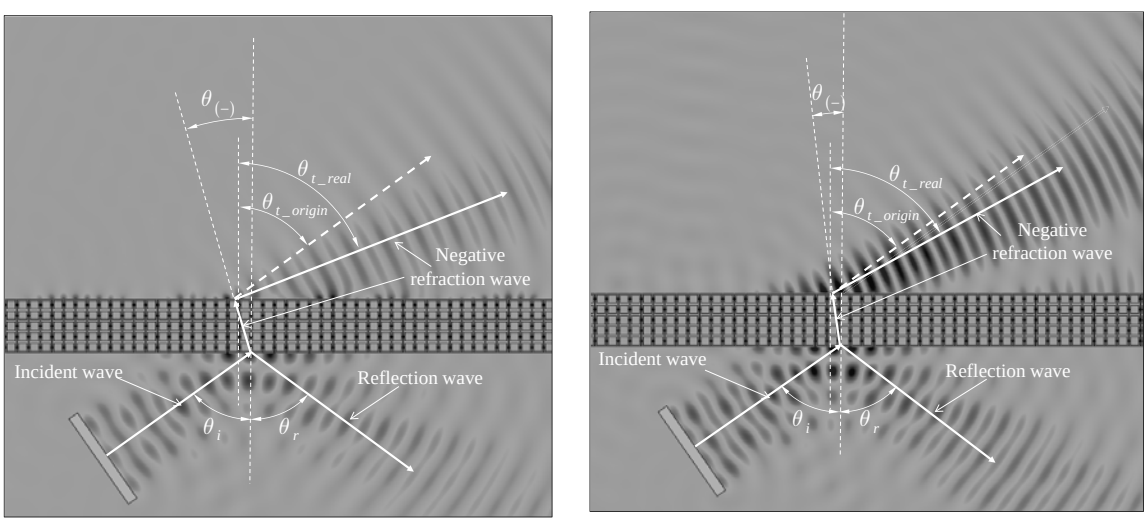

(a) (b)

Fig. 12. Acoustic wave refraction at different excitation frequencies: (a) 2100 Hz and (b) 2300 Hz (the bold arrows represent the wave directions in the actual simulation, and the dotted arrow represents the wave direction expected by Snell's law).

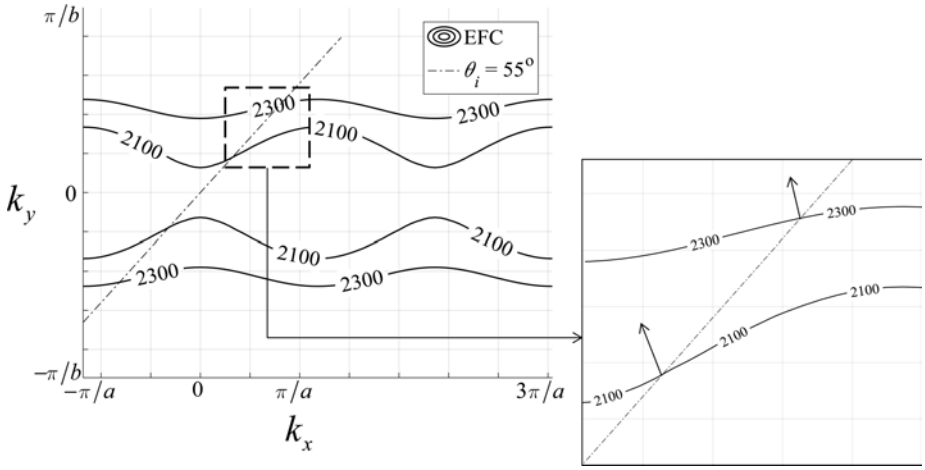

Fig. 13. EFC results at different excitation frequencies. The dotted lines represent the directions of the incident waves. The arrows in the expanded figure of the EFC represent the directions of the diffraction wave.

at 2600 Hz for an incident wave at an angle of 55°. This interesting phenomenon can also be explained by the EFC of Fig. 13. As shown, the negative refraction angles at 2100 Hz and 2300 Hz are −16.7° and −6.8°, respectively, which demonstrate the frequency dependence of the refracted waves.

Based on Snell's law in a homogeneous medium with a circular EFC, the incident and the transmitted angles must always be the same. The present metastructure in Fig. 12 shows how refraction depends on the incident wave angle. Considering the influence of the refractive index and Snell's law, the following small angle formulation can be used to estimate the angle in accordance to,

$$\theta_{\text{t\_real}} = \theta_{\text{t\_origin}} - \theta_1 - \theta_2 \quad \text{and} \quad \theta_{\text{t\_origin}} = \theta_i, \tag{30}$$

where θ_1 and θ_2 are the first and the second refraction angles. From the numerical experiment in Fig. 12(a), θ_1, θ_2, and $\theta_{\text{t\_real}}$, are −16.7°, 2.9°, and 68.8°, respectively. In Fig. 12(b), θ_1, θ_2, and $\theta_{\text{t\_real}}$, are −6.8°, 0.8°, and 61°, respectively.

3.2. *Acoustic metamaterial hyperlens configuration*

Using the metamaterial structure developed in Fig. 6, it is possible to make an arc-shaped acoustic metamaterial hyperlens, as shown in Fig. 15. The dimensions of the unit cells are slightly different, depending on their locations. The present acoustic hyperlens is constructed by stacking 40 layers of unit cells in the radial direction. The number of unit cells in the circumferential direction is the same in all 20 layers. Since the size of the unit cell in the 20th layer is twice the size of the unit cell in the first layer, the number of unit cells in the circumferential direction is doubled from the 21th layer onwards. Because the driven frequency range is defined by the EFC, and the EFC varies depending on the shape of the unit cell, it is necessary to check whether there is a difference in the driving frequency

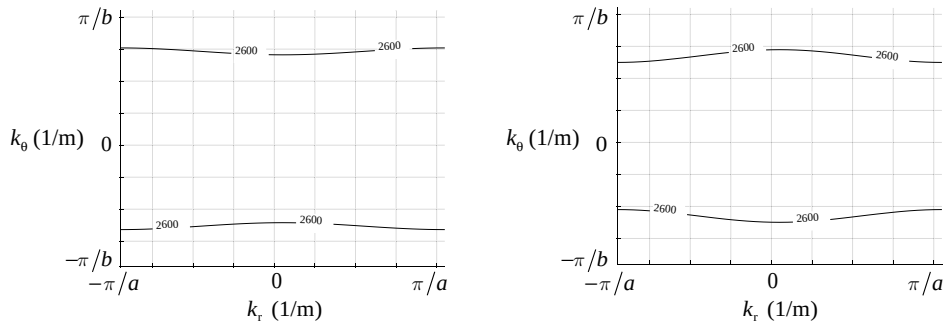

Fig. 14. EFCs of unit cells in the (a) first and (b) 20th layers.

between the EFC of the first layer and the EFC of the 20th layer. The EFC of the unit cell of the first and 20th layers are shown in Fig. 14,

In Fig. 14, the excitation frequency layers of the first and 20th layers are similar. Therefore, the layered acoustic hyperlens can operate at 2600 Hz. In order to test the performance and characteristics of the hyperlens, two-point sound sources are located at the bottom of the arc-shaped acoustic hyperlens. Setting the distances of the point sound sources to be smaller than the diffraction limit, wave propagation phenomena are simulated, and the characteristics of the hyperlens can thus be studied. In this simulation, the diffraction limit is 6.5 cm for 2600 Hz.

In Fig. 15, the parameters of the unit cell should be different in each layer because the circumferential length changes in each layer. To ensure validity of this argument in

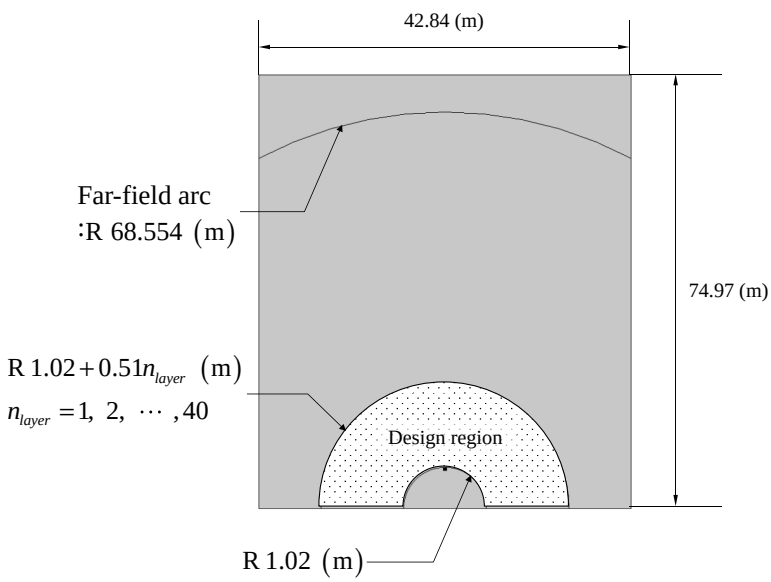

Fig. 15. Dimensions of the acoustic hyperlens region.

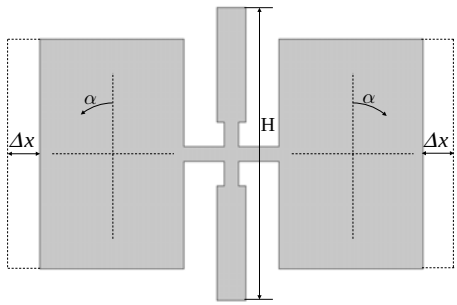

Fig. 16. Parameters of the acoustic hyperlens unit cell in each layer ($H = h_1 + h_4, \Delta x = (n_{\text{layer}} - 1)H \tan\alpha$).

the semicircular annulus of Fig. 15, the unit cells should be curved, and the geometric parameters should be changed accordingly, as shown in Fig. 16.

In Fig. 16, the total height of the unit cell is H, the number of layers is n_{layer}, and the cavity rotation angles on both the left and right sides are equal to $\alpha(= 1.87°)$, respectively. If the number of layers is higher than 20, the rotation angle should be changed to half of its value from the 21st layer onwards.

For the metamaterial analyses, an infinite repeating unit cell is assumed. However, in real engineering applications, a finite unit cell size should be used. To analyze the effect of the number of layers in the acoustic metamaterial, the wave propagation analyses are performed by varying the number of the layers from 3 to 5, as shown in Fig. 15. The acoustic pressure distribution is calculated at the far-field arc of Fig. 15. It is noticed

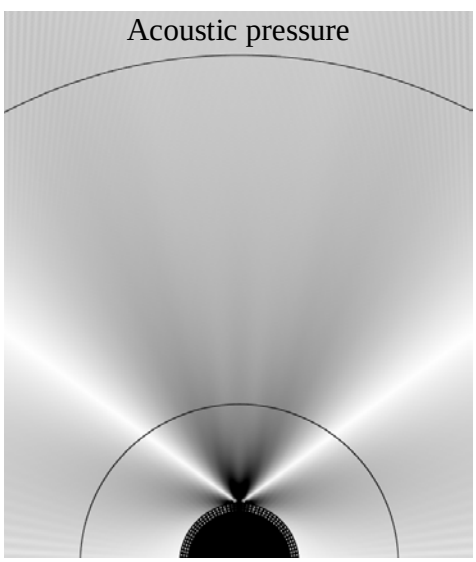

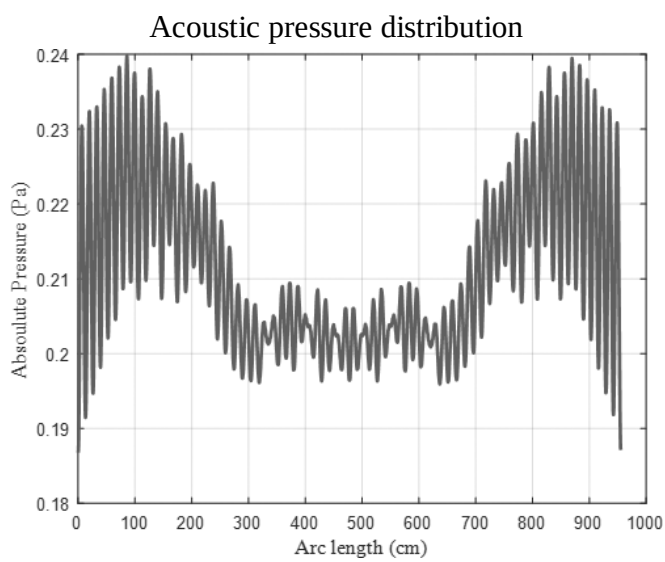

(a)

Fig. 17. Acoustic pressure distributions as a function of the number of DSHS layers. (a) Three layers and (b) five layers.

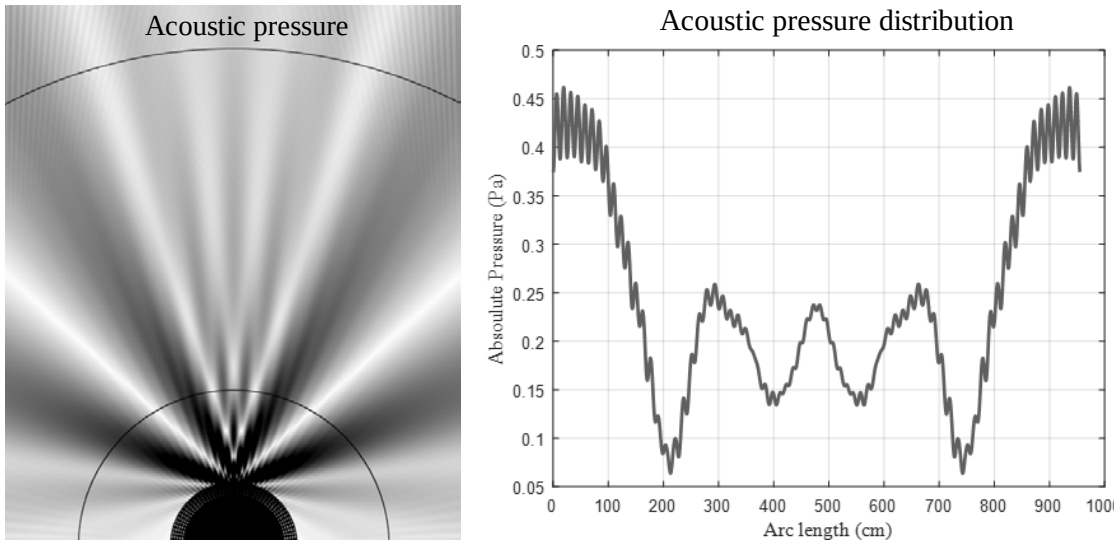

(b)

Fig. 17. (*Continued*)

that owing to the impedance differences, the acoustic pressures of the developed acoustic metamaterial are decreased by increasing the number of layers. It is observed that the ripples of the acoustic wave in the circumferential direction are decreased by increasing the layer numbers.

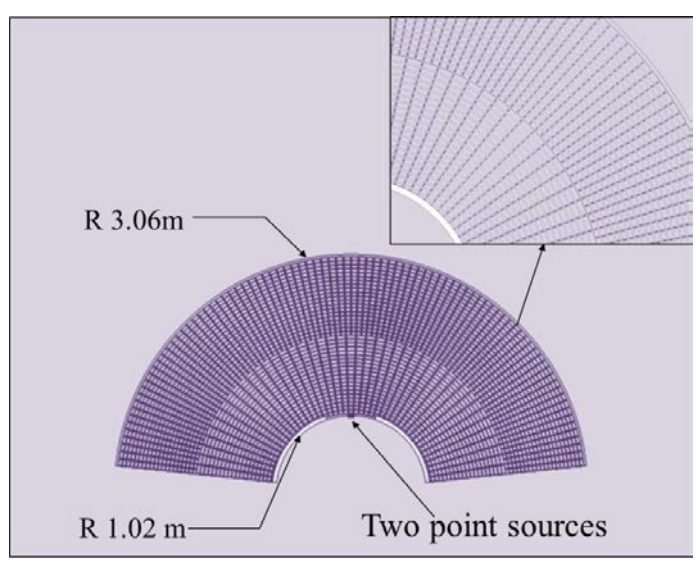

(a)

Fig. 18. Wave propagation results for the two sound sources separated by 2 cm and excited at 2600 Hz. (a) The acoustic wave propagation (a) without and (b) with the hyperlens.

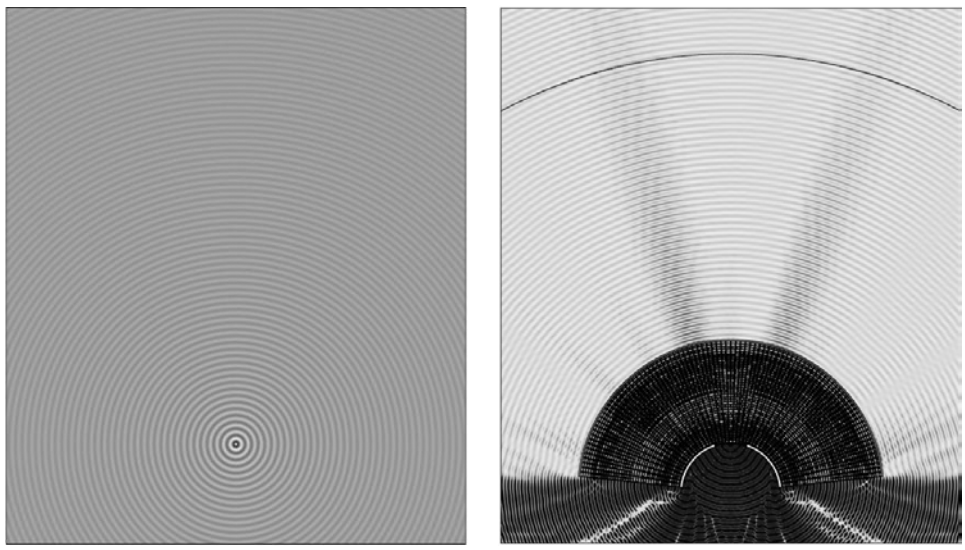

(b) (c)

Fig. 18. (*Continued*)

For the hyperlens application example, Fig. 18 shows the wave separation example with 50 layers using two sound sources separated by 2 cm. Without the hyperlens, the two sources cannot be distinguished, but with the hyperlens they can be separated, as shown. This example shows the potential application of the proposed acoustic metamaterial.

4. Conclusions

This research presented a new acoustic metamaterial using the repeated DSHS structure. A metamaterial offers an interesting solution to overcome the diffraction limit by transforming evanescent waves that allow the imaging of subwavelength features of an object into propagating waves. Therefore, many numerical and experimental studies can be pursued. This research presented a new subwavelength acoustic metamaterial system with repeated DSHS unit cells that elicited an effective negative bulk modulus. According to the dispersion relation, to implement the acoustic hyperlens, one of the wavevectors should be imaginary. To analyze the frequency range in which the wavevector had an imaginary value, a 2D anisotropic mass–spring system was designed. Based on the analyses of this 2D mass–spring system, we identified the frequency range that could represent the performance of the acoustic hyperlens. This 2D mass–spring system was approximated by an acoustic system that was used to implement the acoustic hyperlens. In the process of verifying the performance of such an acoustic hyperlens, we discovered a new refraction phenomenon whereby deviations from Snell's law were documented. Correspondingly, we proposed a new refraction formula that defined the phenomenon based on EFC analyses. To construct the continuous and periodic structure in some sense, the 2D mass–spring lattice was reanalyzed and the two approximations postulated for the metamaterial were carefully realized

in the constructed unit cells of this acoustic metamaterial. The potential applicability of the proposed hyperlens was also presented, and the function of the proposed hyperlens was verified by changing the distance between the two sound sources. The presented acoustic metamaterial can overcome the diffraction limit and can distinguish sound sources that are closer than the diffraction limit in conventional media. Future work will focus on the implementation and manufacturing of the developed metamaterial configuration, while new research will focus on the reduction of the impedance mismatches to decrease damping.

Acknowledgments

This work was supported by the National Research Foundation of Korea (NRF) Grant No. 2014M3A6B3063711 (Global Frontier R & D Program on Center for Wave Energy Control based on Metamaterials) and Grant No. NRF-2015R1A2A2A11027580 funded by the Korean Ministry of Science, ICT, and Future Planning (MSIP).

References

1. R. A. Shelby, D. R. Smith, S. C. Nemat-Nasser and S. Schultz, Microwave transmission through a two-dimensional, isotropic, left-handed metamaterial, *Appl. Phys. Lett.* **78** (2001) 489.
2. R. A. Shelby, D. R. Smith and S. Schultz, Experimental verification of a negative index of refraction, *Science* **292** (2001) 77–79.
3. L. Sun, Experimental investigation of vibration damper composed of acoustic metamaterials, *Appl. Acoust.* **119** (2017) 101–107.
4. T. Wang, M.-P. Sheng, Z.-W. Guo and Q.-H. Qin, Flexural wave suppression by an acoustic metamaterial plate, *Appl. Acoust.* **114** (2016) 118–124.
5. S. Varanasi, J. S. Bolton, T. H. Siegmund and R. J. Cipra, The low frequency performance of metamaterial barriers based on cellular structures, *Appl. Acoust.* **74** (2013) 485–495.
6. A. Bermudez, L. Hervella-Nieto, A. Prieto and R. Rodriguez, Validation of acoustic models for time-harmonic dissipative scattering problems, *J. Comput. Acoust.* **15** (2007) 95–121.
7. G. H. Yoon, Unified analysis with mixed finite element formulation for acoustic-porous-structure multiphysics system, *J. Comput. Acoust.* **23** (2015) 1550002.
8. X. Z. A. Z. LIU, Superlenses to overcome the diffraction limit, *Nat. Mater.* **5** (2006) 452–456.
9. H. J. Lee, H. W. Kim and Y. Y. Kim, Far-field subwavelength imaging for ultrasonic elastic waves in a plate using an elastic hyperlens, *Appl. Phys. Lett.* **98** (2011) 241912.
10. Z. Liang and J. Li, Bandwidth and resolution of super-resolution imaging with perforated solids, *AIP Adv.* **1** (2011) 041503.
11. M. Ambati, N. Fang, C. Sun and X. Zhang, Surface resonant states and superlensing in acoustic metamaterials, *Phys. Rev. B* **75** (2007).
12. J. Li, L. Fok, X. Yin, G. Bartal and X. Zhang, Experimental demonstration of an acoustic magnifying hyperlens, *Nat. Mater.* **8** (2009) 931–934.
13. T.-Y. Chiang, L.-Y. Wu, C.-N. Tsai and L.-W. Chen, A multilayered acoustic hyperlens with acoustic metamaterials, *Appl. Phys. A* **103** (2011) 355–359.
14. S. Guenneau, A. Movchan, G. Pétursson and S. Anantha Ramakrishna, Acoustic metamaterials for sound focusing and confinement, *New J. Phys.* **9** (2007) 399–399.
15. Z. G. Wang, S. H. Lee, C. K. Kim, C. M. Park, K. Nahm and S. A. Nikitov, Acoustic wave propagation in one-dimensional phononic crystals containing Helmholtz resonators, *J. Appl. Phys.* **103** (2008) 064907.

16. X. Ao and C. T. Chan, Far-field image magnification for acoustic waves using anisotropic acoustic metamaterials, *Phys. Rev. E*: *Stat Nonlinear Soft Matter Phys.* **77** (2008) 025601.
17. A. B. Movchan and S. Guenneau, Split-ring resonators and localized modes, *Phys. Rev. B* **70** (2004) 125116.
18. J.-B. Li, Y.-S. Wang and C. Zhang, Tuning of Acoustic Bandgaps in Phononic Crystals With Helmholtz Resonators, *J. Vib. Acoust.* **135** (2013) 031015.
19. A. Alberti, I. Spiousas, P. M. Gomez, M.C. Eguia, Resonance switching in a large sonic crystal cavity, *Appl. Acoust.* **116** (2017) 390–393.
20. B. S. Beck, N. H. Schiller and M. G. Jones, Impedance assessment of a dual-resonance acoustic liner, *Appl. Acoust.* **93** (2015) 15–22.
21. X. Y. Xiao and R. P. Chen, Acoustic band gap extension in one-dimensional solid/fluid phononic crystal heterostructure, *J. Comput. Acoust.* **22** (2014) 1450010.
22. M. S. Fokina and V. N. Fokin, Resonances of acoustic waves interacting with an elastic seabed, *J. Comput. Acoust.* **9** (2001) 1079–1093.
23. B. Xia, N. Chen, L. Xie, Y. Qin and D. Yu, Temperature-controlled tunable acoustic metamaterial with active band gap and negative bulk modulus, *Appl. Acoust.* **112** (2016) 1–9.
24. A. Lipson, S. G. Lipson and H. Lipson, *Optical Physics* (Cambridge University Press, 2010).
25. A. Poddubny, I. Iorsh, P. Belov and Y. Kivshar, Hyperbolic metamaterials, *Nat. Photon.* **7** (2013) 948–957.
26. D. Lu and Z. Liu, Hyperlenses and metalenses for far-field super-resolution imaging, *Nat. commun.* **3** (2012) 1205.
27. J. B. Pendry, Negative refraction makes a perfect lens, *Phys. Rev. Lett.* **85** (2000) 3966.
28. Z. Liu, C. T. Chan and P. Sheng, Analytic model of phononic crystals with local resonances, *Phys. Rev. B* **71** (2005) 014103.
29. H. H. Huang and C. T. Sun, Wave attenuation mechanism in an acoustic metamaterial with negative effective mass density, *New J. Phys.* **11** (2009) 013003.
30. H. H. Huang, C. T. Sun and G. L. Huang, On the negative effective mass density in acoustic metamaterials, *Int. J. Eng. Sci.* **47** (2009) 610–617.
31. S. Yao, X. Zhou and G. Hu, Experimental study on negative effective mass in a 1D mass–spring system, *New J. Phys.* **10** (2008) 043020.
32. S. H. Lee, C. M. Park, Y. M. Seo, Z. G. Wang and C. K. Kim, Acoustic metamaterial with negative density, *Phys. Lett. A* **373** (2009) 4464–4469.
33. N. Fang, D. Xi, J. Xu, M. Ambati, W. Srituravanich, C. Sun and X. Zhang, Ultrasonic metamaterials with negative modulus, *Nat. Mater.* **5** (2006) 452–456.
34. A. Mar-Or and D. Givoli, A finite element structural-acoustic model of coupled membranes, *J. Comput. Acoust.* **12** (2004) 605–618.
35. C. Ding, H. Chen, S. Zhai and X. Zhao, Acoustic metamaterial based on multi-split hollow spheres, *Appl. Phys. A* **112** (2013) 533–541.
36. Z. Jacob, L. V. Alekseyev and E. Narimanov, Optical hyperlens: Far-field imaging beyond the diffraction limit, *Opt. Exp.* **14** (2006) 8247–8256.